The axisymmetric and plane cases of a gas phase steadily displacing a Newtonian liquid—A simultaneous solution of the governing equations

María D. Giavedoni and Fernando A. Saita
Instituto de Desarrollo Tecnológico para la Industria Química (INTEC), Universidad Nacional del Litoral, CONICET, Güemes 3450 (3000), Santa Fe, Argentina

(Received 7 January 1997; accepted 10 April 1997)

The flow induced by a long bubble steadily displacing a liquid confined by two closely located parallel plates or by a cylindrical tube of small diameter is numerically analyzed. The technique employed solves the complete set of governing equations simultaneously. The present analysis encompasses, and also extends, the whole range of Capillary values previously studied with various numerical techniques. The results shown uncover a type of recirculating flow pattern that appears to have been overlooked before. The effects of the inertial forces on the liquid flow rate are also assessed. © *1997 American Institute of Physics.* [S1070-6631(97)01408-6]

I. INTRODUCTION

The gas–liquid displacement in a capillary tube or in the gap between two closely spaced parallel plates is commonly employed as a model to analyze multiphase systems. One important example is found in enhanced oil recovery.

When the length of the gas phase is somewhat larger than the distance between the solid walls, a stagnant layer of fluid covering the walls is left behind the moving front; in the limit of low velocity ($Re=0$), the thickness of the film formed is a function of the Capillary number alone. In their pioneer study, Fairbrother and Stubbs[1] found an empirical correlation between the film thickness (h_∞) and the Capillary number (Ca) valid in the range $10^{-3}\leqslant Ca\leqslant 10^{-2}$. Measuring the fraction of liquid (m) left on the wall of a capillary tube, Taylor[2] extended this range for Ca up to 10^{-1} and he also reported that the film thickness reaches a limiting value as the Capillary number increases. Bretherton,[3] on the assumption that the lubrication approximation is valid in the transition region between the front of the moving interface and the film region, was the first to study the problem theoretically for vanishing Capillary number. He derived expressions correlating the thickness of the film and the pressure drop across the bubble with Ca. His experimental measurements of h_∞ compare well with his theoretical predictions if the Capillary number is in the range 10^{-2}–10^{-3}, but a systematic deviation is observed for lower values of Ca. This deviation could be due to the effects of surfactants present in very small amounts.

Using a conductimetric technique, Chen[4] observed that the film thickness monotonically decreases as the Capillary number decreases until it approaches a constant value at low Ca; that is, he reported the same deviation observed by Bretherton and he presented evidence that it could be due to the roughness of the tube wall. The approach of Bretherton[3] was formalized by Park and Homsy[5] with the use of perturbation theory and matched asymptotic expansions, and it was extended by Ratulowski and Chang[6] to higher Capillary values using an arclength formulation of a composite lubrication equation.

For values of Ca larger than 5×10^{-3} numerical studies are required. To analyze the displacement of a liquid by a semi-infinite bubble, Reinelt and Saffman[7] used finite differences combined with two different grids, one curvilinear conformal to the interface and the other rectilinear parallel to the solid boundaries. They considered two flow geometries: plane and axisymmetric, in both cases their results were in good agreement with experiments if $10^{-2}\leqslant Ca\leqslant 2$.

Shen and Udell[8] presented a finite element solution of the axisymmetric problem for $Re=0$ and $5\times 10^{-3}\leqslant Ca\leqslant 0.2$. For Capillary numbers greater than 0.2 the free surface profiles showed oscillations probably due to a deficient resolution of the flow field near the bubble front. They found results in very good agreement with the predictions of both Bretherton's theory at low Ca and the empirical correlation of Fairbrother and Stubbs in the range: $10^{-2}\leqslant Ca\leqslant 0.1$.

Lu and Chang[9] used the boundary integral method to analyze a long bubble displacing a liquid initially confined between two parallel plates. They considered the leading edge of the gas phase and obtained solutions for Capillary numbers as small as 5×10^{-4}, the lower limit at which numerical solutions of this problem are available, and up to $Ca=1$. For low Ca (10^{-2} or smaller), their reported values of the film thickness are in good agreement with those of Bretherton's lubrication analysis and with Reinelt and Saffman's numerical results. However, the agreement for the pressure drop across the interface at the bubble front is less satisfactory.

The study performed by Shen and Udell[8] was extended by Martinez and Udell.[10] In fact, using a boundary integral method they considered the leading and trailing meniscus of a long bubble moving steadily in a capillary tube filled with a viscous fluid. They reported film thickness and pressure drop values that are in good agreement with published results in the range $10^{-2}\leqslant Ca\leqslant 10$ for the leading meniscus and $10^{-2}\leqslant Ca\leqslant 1.5$ for the trailing meniscus.

Martinez and Udell[11] and Tsai and Miksis[12] analyzed the axisymmetric creeping flow problem using the boundary integral method. They integrated the kinematic condition to march in time from an assumed initial bubble shape until the final steady state was attained. However, this equation be-

 1070-6631/97/9(8)/2420/9/$10.00

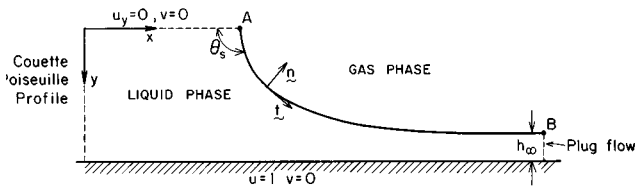

FIG. 1. Schematic representation of the steady translation of a gas phase in a liquid and the coordinate system adopted.

comes stiff in the regions where a thin film separates the bubble from the tube walls; thus the method is successful provided the bubble is not too long and the Capillary number is not too small. They presented solutions for $Ca \geqslant 0.05$ and for bubbles whose initial undeformed radius were equal to or smaller than 1.2 r_o (r_o is the tube radius).

In this work the steady displacement of a viscous fluid by a semi-infinite gas bubble is numerically analyzed in the two geometries previously considered by Reinelt and Saffman,[7] that is parallel plates and cylindrical tubes. The numerical technique here adopted simultaneously solves the equation that governs the free surface shape and the system of nonlinear equations arising from the flow field; therefore the solution of the problem is obtained in a single step. This technique was formerly developed by Ruschak[13] and later improved by Saito and Scriven[14] and Kistler and Scriven.[15] It uses the finite element method combined with a suitable parametrization of the free surface.

The solutions to be presented in Sec. IV pertain to the leading front of a semi-infinite bubble. The simultaneous approach employed here yields results that encompasses all previously published numerical solutions of this problem. In fact, our results are for Ca between 5×10^{-5} and 10 which enlarges the range of Capillary numbers analyzed up to date. Computed values of the liquid film thickness and of the pressure drop across the ''bubble'' front are in excellent agreement with published results.

Computed streamlines show how the flow field changes when the Capillary number is varied and they make evident the existence of two different recirculating flow patterns; apparently, one of them has been overlooked in the analyses previously published. The results also show approximately at which Capillary value the transition from one recirculating flow pattern to the other occurs.

Finally, since the inertial forces can be computed with negligible additional cost, their effects on the liquid flow rate are examined too.

II. GOVERNING EQUATIONS

We consider the steady movement of an inviscid gas in both a capillary tube of radius d and between two closely spaced parallel plates separated a distance $2d$, displacing an incompressible Newtonian liquid of constant viscosity μ and density ρ, as shown in Fig. 1. The gas is translating steadily with speed U, its pressure is uniform everywhere and it exerts only normal stresses on the interface; the value of the gas pressure (which is arbitrarily set equal to zero) is used as the pressure datum of the two phase system. Gravitational forces are neglected since the characteristic distance (d) is small. The bubble is moving along the axis of the tube or the centerline of the channel, so the flow is symmetric about $y=0$. Under these conditions, the mass balance in the liquid is described by the continuity equation

$$\nabla\cdot\mathbf{v}=0, \tag{1}$$

and the momentum balance by the Navier–Stokes equation

$$Re\ \mathbf{v}\cdot\nabla\mathbf{v}=\nabla\cdot\mathbf{T},\quad \mathbf{T}=-\frac{p}{Ca}\mathbf{I}+[\nabla\mathbf{v}+(\nabla\mathbf{v})^T]. \tag{2}$$

Equations (1) and (2) are in their dimensionless form. The characteristic scales used are the distance d and the gas phase speed U. Pressure and stresses are measured in units of capillary force (σ/d, σ is the liquid–air surface tension), $Re=\rho Ud/\mu$ is the Reynolds number, and $Ca=\mu U/\sigma$ is the Capillary number.

Equations (1) and (2) are solved considering a coordinate system that moves with the gas phase. In this reference frame, the appropriate boundary conditions are stated next.

(i) On the solid wall the liquid adheres to the solid, then

$$u=1,\ v=0;\ y=1,\ 0\leqslant x<\infty. \tag{3}$$

(ii) At the centerline, we impose symmetry conditions

$$u_y=0,\ v=0;\ y=0,\ 0\leqslant x<x_{FS} \tag{4}$$

except for $x=x_{FS}$ where $\mathbf{v}=\mathbf{0}$.

(iii) Far upstream the flow is one-dimensional; consequently, the velocity distribution should be parabolic satisfying the boundary conditions (3) and (4), i.e.,

$$u=-(1-h_\infty)(1-y^2)\left[\frac{3}{2}\alpha+2\beta(1-h_\infty)\right]+1,\ v=0, \tag{5}$$

where $\alpha=1$, $\beta=0$ for plane flow and $\alpha=0$, $\beta=1$ for axisymmetric flow. In Eq. (5) h_∞ is the dimensionless thickness of the stagnant liquid film left behind by the moving gas front, this quantity is an unknown which is determined as part of the solution. For the plane case ($\alpha=1$, $\beta=0$) Eq. (5) shows that at the symmetry line the liquid velocity (u) is negative when $h_\infty<1/3$, indicating that ahead of the bubble there exists a recirculating flow. A similar situation occurs for the axisymmetric case ($\alpha=0$, $\beta=1$) when $(1-h_\infty)^2$ is greater than 0.5.

(iv) At the gas–liquid interface the conditions to be satisfied are

$$\mathbf{v}\cdot\mathbf{n}=0, \tag{6}$$

$$\mathbf{T}\cdot\mathbf{n}=\frac{1}{Ca}\left(\frac{1}{R_1}+\frac{1}{R_2}\right)\mathbf{n}. \tag{7}$$

In Eq. (7), R_1 and R_2 are the principal radii of curvature of the interface; then, R_2 which is infinity for the plane case, becomes equal to $y_{FS}/(-\mathbf{n}\cdot\mathbf{e}_y)$ for the axisymmetric case. On the other hand, $\mathbf{n}/R_1=d\mathbf{t}/ds$ in both cases; in this equation $\mathbf{n}$ is the unit normal to the free surface outwardly directed from the liquid phase and $\mathbf{t}$ is the unit tangent to the interface in the direction of increasing arclength (s). The position and the slope of the interface at the stagnation

point—actually a stagnation line for the plane case—($y=0$, $x=x_{FS}$) as well as its slope at $x=\infty$ are specified, but the problem is not overconstrained because h_∞, and consequently the flow rate, is unknown.

(v) As $x\to\infty$ the free surface becomes parallel to the solid wall and is located at a distance h_∞ from it; thus, the flow in that region is rectilinear. There we impose the traction normal to the outflow boundary

$$\mathbf{T}\cdot\mathbf{n}=\frac{\mathbf{n}}{CaR_2};\quad x\to\infty,\quad 1-h_\infty\leqslant y\leqslant 1. \tag{8}$$

In the next section we discuss the more salient features of the numerical technique employed to solve the problem.

III. NUMERICAL PROCEDURE

The numerical technique employed is based on a Galerkin/finite element discretization of the governing equations. Mixed interpolation is used to approximate the flow field on quadrilateral elements with nine-node biquadratic basis functions (Φ^i) for velocity and four-node bilinear ones (Ψ^j) for pressure. These basis functions are built in Cartesian coordinates (ξ,η) on a standard unit square ($0\leqslant\xi,\eta\leqslant 1$); thus we have

$$\mathbf{v}=\sum_{i=1}^{9}\mathbf{v}^i\Phi^i(\xi,\eta), \tag{9}$$

$$p=\sum_{j=1}^{4}p^j\Psi^j(\xi,\eta). \tag{10}$$

The free surface is parametrized by means of spines as suggested by Kistler and Scriven[15] and the coefficients (h) representing the location of the interface are interpolated with the one-dimensional specialization of the biquadratic functions (Φ^i)

$$h=\sum_{i=1}^{3}h^i\Phi^i(\xi,\eta=1). \tag{11}$$

Each quadrilateral element of the flow domain is mapped isoparametrically onto the standard unit square in Cartesian coordinates by means of the nine biquadratic basis functions used in the expansion of the velocity,

$$\mathbf{x}(\xi,\eta)=\sum_{j=1}^{9}\mathbf{x}^j(\mathbf{h})\Phi^j(\xi,\eta), \tag{12}$$

where $\mathbf{x}^j(\mathbf{h})$ are the nodal coordinates which depend on the vector $\mathbf{h}$ whose components are the coefficients of the free surface parametrization.

In Fig. 2 the principal features of the finite element mesh used are illustrated; elements located in (a) are rectangles with fixed coordinates while elements located in (b) and (c) have two curvilinear sides that change with the interface and two straight sides determined by spines. The spines in (b) pass through the point (x_P,0) and their base points and directions are fixed while spines in (c) are perpendicular to the solid wall and their base points can translate along it when the position of the stagnation point (E)—actually a stagnation line—is followed. This last characteristic, i.e., the adjusting of the mesh with the location of the stagnation point E which appears at low values of the Capillary number, is adopted to improve the computational efficiency, since a local refinement near E is needed for a suitable determination of the free surface velocities in that region. Therefore, the mesh coordinates in (c) depend not only on the vector $\mathbf{h}$ [see Eq. (12)] but also on the location of the stagnation point E.

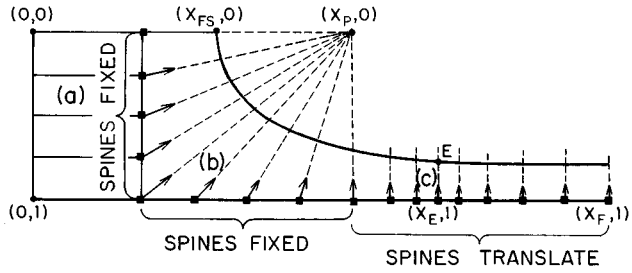

FIG. 2. Schematic representation of the free surface parametrization adopted.

The governing equations (1) and (2) are weighted with the basis functions employed to interpolate the pressure and velocity fields, respectively; then they are integrated in the flow domain. When dealing with the axisymmetric problem, we use the proper formulation derived for a system in cylindrical coordinates (Crochet *et al.*[16]). Equation (6) is weighted with the basis functions used to interpolate the coefficients that locate the free surface and then it is integrated along the interface. This procedure yields the following vanishing residuals:

$$R_C^i=\int_{\Omega_o}\Psi^i[(\alpha+\beta y)(u_x+v_y)+\beta v]Jd\xi d\eta=0, \tag{13}$$

$$\mathbf{R}_M^j=\int_{\Omega_o}(\Phi^j Re\ \mathbf{v}\cdot\nabla\mathbf{v}+\nabla\Phi^j\cdot\mathbf{T})(\alpha+\beta y)Jd\xi d\eta - \int_{\Gamma}\Phi^j\mathbf{T}\cdot\mathbf{n}(\alpha+\beta y)ds=0, \tag{14}$$

$$R_K^k=\int_{FS}\Phi^k\mathbf{v}\cdot\mathbf{n}(\alpha+\beta y)ds=0. \tag{15}$$

In Eqs. (13) and (14) J stands for the Jacobian of the coordinate transformation. In Eq. (14) we have applied the divergence theorem on the diffusive momentum term; therefore natural boundary conditions (7) and (8) can easily be imposed. In the momentum residuals pertaining to the gas–liquid interface the traction vector in the integral along the boundary is replaced by Eq. (7) and the resulting expression is integrated by parts following the procedure suggested by Ruschak.[13] Thus we obtain

$$-\int_{FS}\Phi^j\mathbf{T}\cdot\mathbf{n}(\alpha+\beta y_{FS})ds$$

$$=\frac{1}{Ca}\int_{FS}\mathbf{t}\frac{d}{ds}[\Phi^j(\alpha+\beta y_{FS})]$$

$$+\frac{\beta}{Ca}\int_{FS}\mathbf{n}n_y\Phi^j ds-\frac{1}{Ca}[\Phi^j\mathbf{t}(\alpha+\beta y_{FS})]_A^B. \qquad (16)$$

The symmetry point A is a stagnation point, there we replace the momentum residuals by the corresponding essential boundary condition at that point, i.e., $\mathbf{v}=\mathbf{0}$. The slope of the interface ($\mathbf{t}=\mathbf{e}_x$) is imposed as a boundary condition at point B (x_F, y_{FS}). In Eq. (16), y_{FS} is the radial location of the free surface and n_y is the y component of the unit vector normal to the free surface.

The essential boundary conditions given by Eqs. (3)–(5) directly replace the momentum weighted residuals at the boundary nodes where those equations apply. In order to evaluate h_∞ we must incorporate the symmetry condition at point A into the set of equations; that is $\theta_s=\pi/2$ which is equivalent to $x_\xi=0$ in our numerical code. Finally, when one spine is made to follow the location of the stagnation point (E) we impose

$$u=0;\ x=x_E,\ y=y_{FS} \qquad (17)$$

and the x component of the momentum residual at this node is used to evaluate x_E. The resulting set of nonlinear algebraic equations is simultaneously solved starting with Newton's method and switching to a quasi-Newton iteration when the norm of the difference between two consecutive Newton's steps does not exceed 10^{-2}. The convergence criterium adopted is that the norm of the difference between two consecutive approximations is equal to or smaller than 10^{-6}.

The convergence of the solution was tested varying the density of the mesh and the location of the outflow and inflow boundaries. For low Ca, better results are obtained when one spine follows the location of the stagnation point (E) and the mesh is refined in its neighborhood. In fact, at low Ca the transition zone in which the free surface relaxes to its final height is short and the stagnation point (E) is located almost in the film region; consequently, the interfacial velocity varies from zero at the stagnation point to its maximum value of one, in a very short distance. The mesh described above is able to follow this change appropriately.

Newton's method needs good initial estimates to achieve convergence; once a solution is obtained we employ zero-order continuation when either the Reynolds or the Capillary numbers are modified. The continuation scheme was initiated at large values of Ca and $Re=0$ and no more than 3 or 4 full Newton iterations were required to achieve the criterium adopted to start the quasi-Newton iteration process.

The strategy just described, i.e., the simultaneous solution of the complete set of equations and boundary conditions, is one of the features that distinguishes the present work from its predecessors. In fact, most of the previous analyses[7–10] were performed using a two-steps iterative scheme which can be summarized as follows:

TABLE I. Adopted limit values for physical properties of the fluids and characteristics variables of the system.

$U=10^{-3}$–0.3 m/s
$\sigma=15\times10^{-3}-75\times10^{-3}$ N/m
$\mu=10^{-3}-10^{-1}$ Pa s
$d=0.5\times10^{-3}-10^{-3}$ m
$\rho=10^3$ kg/m^3

(i) Equations (1) and (2) are solved in a prescribed domain with one of the free surface boundary conditions omitted. Usually the boundary condition chosen is the kinematic condition [Eq. (6)] or the normal stress condition [Eq. (7)] depending upon whether the Capillary number is larger or smaller than one, respectively.

(ii) The boundary condition set aside in step one is here used to adjust the shape of the gas–liquid interface.

If the process converges, these two steps are repeated until the desired agreement is reached. However, as Silliman and Scriven[17] pointed out, there are cases in which the performance of the process is poor or it does not converge at all regardless of which boundary condition is employed. Another strategy used by several authors[11,12] was to solve a transient problem evolving in time by means of the kinematic condition; in this case a previously converged result for a given Capillary number is used as initial condition to seek the solution for a nearby Capillary value. This methodology requires an increasing number of time steps for smaller Ca, being inappropriated for low values of this parameter.

IV. FINITE ELEMENT SOLUTIONS

Finite element solutions were obtained in both geometries for Capillary numbers ranging between 5×10^{-5} and 10, and Reynolds numbers between 0 and $Re_{max}(Ca)$. The corresponding value of Re_{max} for a particular Ca is calculated assuming that the physical properties of the fluids and the characteristic variables of the system take on the values reported in Table I. The mesh used to compute these solutions has 140 elements with 49 free surface nodes; differences in the value of the final film thickness obtained with a much more refined mesh (191 elements and 63 free surface nodes) do not exceed 0.06%.

The numerical calculations were performed by a Digital Alpha 1000 computer, for the aforementioned more refined mesh a complete iteration using Newton's method took about 40 s of CPU time.

In what follows we first present solutions of the creeping flow problem in the two geometries, plane and axisymmetric, and we compare our solutions with results previously reported in the literature. Then we examine the different flow patterns occurring in the system when the Capillary number is changed and finally we analyze the effects of the inertial forces on h_∞.

A. Creeping flow regime

1. Film thickness and pressure drop predictions

Figures 3(a) and 3(b) illustrate the computed values of h_∞ (plane case) and $m=1-(1-h_\infty)^2$ (axisymmetric case) as

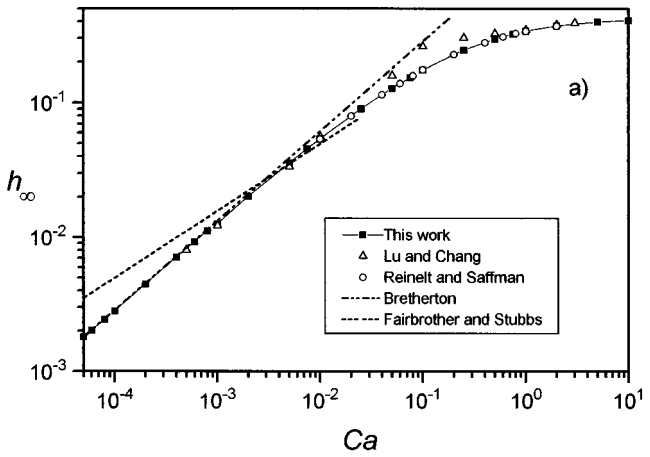

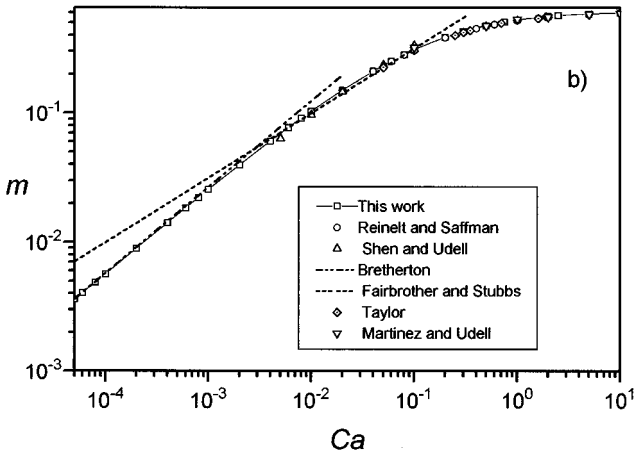

FIG. 3. (a) Film thickness predictions as a function of the Capillary number (plane flow). (b) Film thickness parameter (m) as a function of the Capillary number (axisymmetric flow).

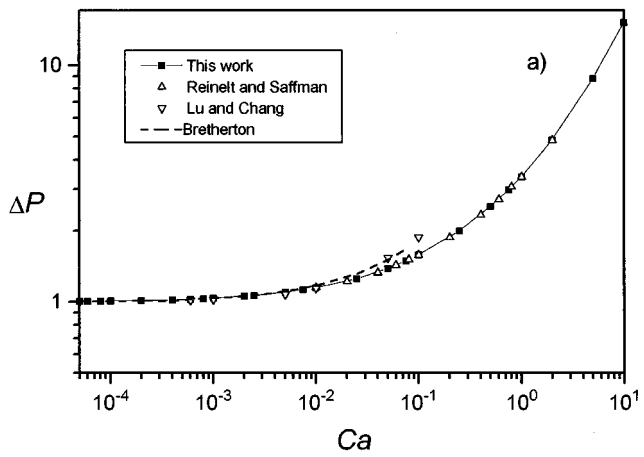

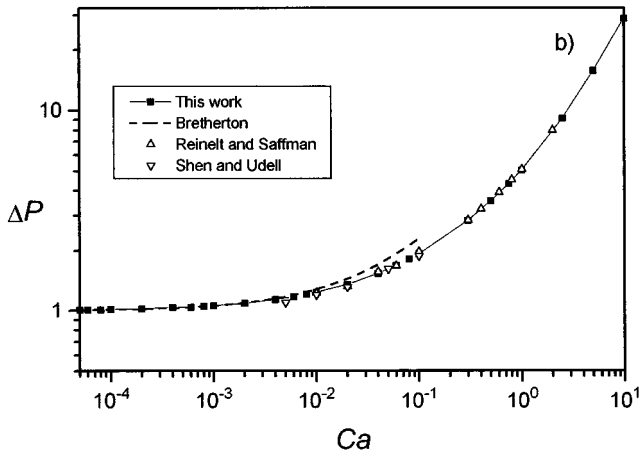

FIG. 4. (a) Pressure drop between points B and A as a function of Ca (plane flow). (b) Pressure drop between points B and A as a function of Ca (axisymmetric flow).

a function of Ca, respectively; we have also plotted previously published results for comparison. It can be observed that for $Ca<10^{-3}$ our results match the theoretical correlation of Bretherton ($h_\infty=1.3375Ca^{2/3}$) while for larger Capillary numbers there is a significant deviation from it. In fact, for $Ca=10^{-4}$ the differences do not exceed 1.8% while for $Ca=10^{-2}$ the differences are about 12%. This is an expected result because Bretherton's analysis is valid for very low velocities (i.e., vanishing Ca). Values of h_∞ reported here are in good agreement with the finite difference solutions of Reinelt and Saffman[7] and with the boundary integral results of Lu and Chang;[9] however, Reinelt and Saffman's and our predictions deviate from those of Lu and Chang in the range of Capillary numbers between 0.01 and 0.8. It is important to mention that a comparison of our values of $(1-h_\infty)$ with those of Reinelt and Saffman, for six different Capillary numbers, shows a maximum difference of 0.12% and a mean difference of 0.06%.

The fraction of liquid left on the tube wall (m) evaluated with the present numerical technique agrees very well with the experimental observations of Taylor[2] as well as with the numerical solutions of Reinelt and Saffman,[7] Shen and Udell,[8] and Martinez and Udell.[10] Also in this case we have compared our values of $(1-h_\infty)$ with those of Reinelt and Saffman for ten Capillary values; the comparison gave a maximum difference of 0.53% and a mean difference of 0.167%. As pointed out by Taylor,[2] m approaches an asymptotic value at large Ca; our computations give $m=0.559$ at $Ca=2$ (Taylor's result is 0.55) and $m=0.592$ at $Ca=10$, a result in agreement with the value computed by Martinez and Udell[10] and with the experimental measurements of Cox.[18] The final film thickness attains a value of 0.361 at $Ca=10$ indicating that only 40% of the liquid originally contained in the tube is displaced by the advancing gas.

The pressure drop between the points defined in Fig. 2 as A and B (ΔP) versus Ca is presented in Figs. 4(a) and 4(b) for the plane and axisymmetric geometries, respectively. Previous results are also plotted for comparison. It is evident that our numerical solution is the one that better matches the asymptotic solution of Bretherton at low Capillary number. For $Ca>0.01$, and for the plane geometry the agreement with the two-dimensional results of Reinelt and Saffman[7] is very good while there is no coincidence with the results reported by Lu and Chang.[9] It should be noticed that the pressure is the least accurate variable in Lu and Chang's study because it is determined from the local curvature at the bubble front.

The values of the pressure drop corresponding to the axisymmetric case [Fig. 4(b)] are in excellent agreement with the finite-difference solutions of Reinelt and Saffman[7]

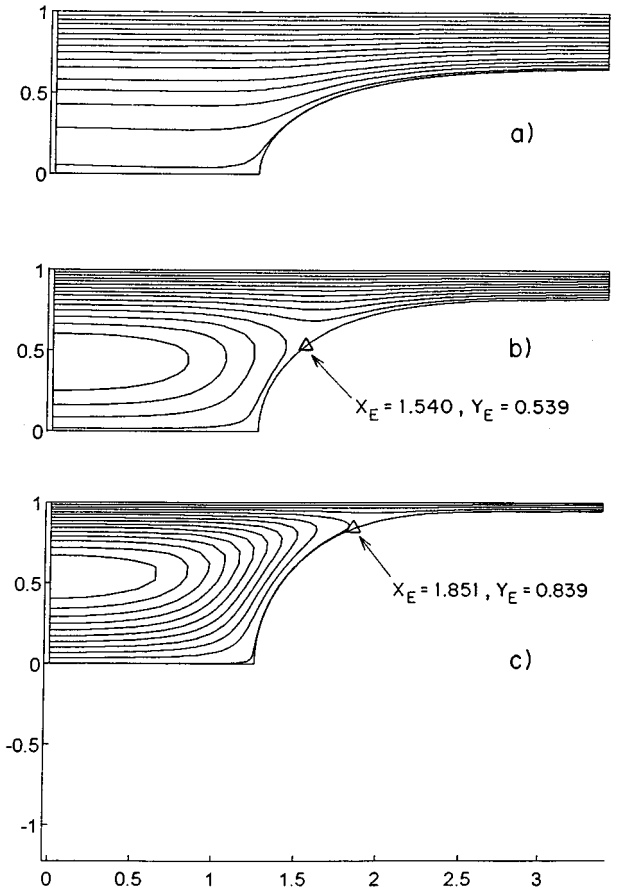

FIG. 5. Computed streamlines for plane flow: (a) $Ca=1$, (b) $Ca=0.1$, (c) $Ca=0.01$.

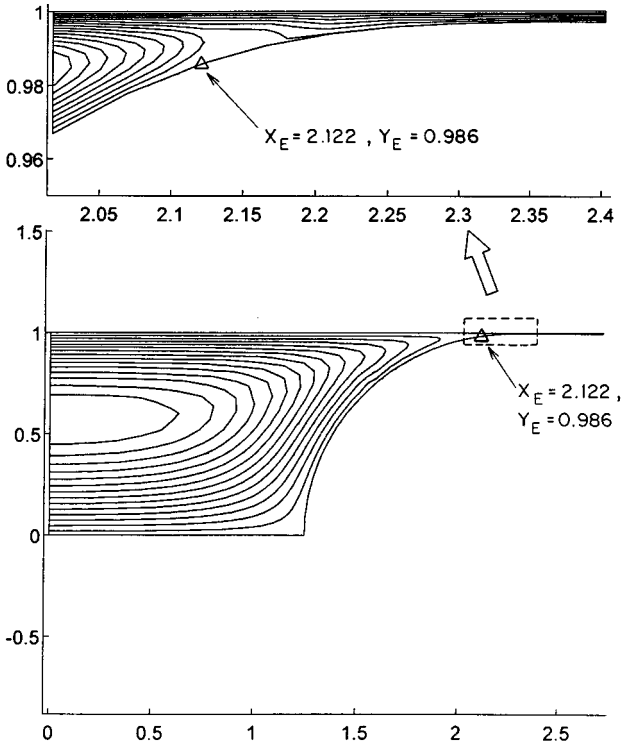

FIG. 6. Computed streamlines for plane flow and $Ca=10^{-4}$.

and they slightly differ from the finite element results of Shen and Udell.[8] As pointed out by Martinez and Udell,[10] at low Capillary numbers surface tension effects are very important, consequently the appropriate scale for pressure is (σ/d); for $Ca>1$ viscous effects are dominant and in this case the appropriate scale for pressure is $(\mu U/d)$. The asymptotic appearance observed in Fig. 4 results from the use of the first scale in the complete range of Ca. It should be emphasized that the technique presented here is able to solve the problem in a range of Capillary numbers which was previously covered with different methodologies; moreover, we have been able to solve the problem at lower values of Ca.

2. Flow field predictions

The streamlines portrayed in this work pertain to the plane case; those corresponding to the axisymmetric geometry are not shown since they are qualitatively similar.

Figure 5 presents the streamlines obtained for three different Capillary values: 1, 0.1, and 0.01; it shows as a remarkable feature the recirculating flow pattern which is already established when $Ca=0.1$ and becomes stronger as the Capillary number is reduced. Elementary calculations based on Eq. (5) indicate that a liquid backflow region must appear when h_∞ is less than 1/3 for the plane case and when m is less than 1/2 for the axisymmetric case; Fig. 5(a) for $Ca=1$ is just an example of a flow pattern without recirculation.

The leading front of the bubble, which appears rather elongated when $Ca=1$, tends to adopt the shape of an arc of circle as the Capillary number diminishes. This behavior is clearly depicted in Figs. 5(b) and 5(c) and is emphasized in Fig. 6 which shows an almost perfect arc of circle of 90° when $Ca=10^{-4}$. These observations are similar to those previously reported by several authors.[7–9]

When there is no recirculating flow as in the case shown in Fig. 5(a), there exists a single stagnation point just at the vertex of the meniscus (actually, a stagnation line for the plane case). For the cases exemplified in Figs. 5(b), 5(c), and 6 there are additional stagnation lines on the interface: two in the plane case and a single stagnation ring in the axisymmetric case. As the Capillary number is reduced these stagnation lines move away from the symmetry line and approach the confining walls; this phenomenon occurs in both geometries.

Figure 6 exemplifies the case where the stagnation line is located close to the wall and also close to the point where the gas–liquid interface relaxes to its final height; thus, the interfacial velocity changes from zero to one in a very short distance and a fine tessellation is needed there to solve the velocity field properly. This is the reason why we use in that zone a fine mesh that moves along with the stagnation line.

Figure 7 shows the values of h_∞ and m when the Capillary number changes between 0.2 and 1.0. According to this plot the recirculating flow region for the axisymmetric case appears when the Capillary number is about 0.7. By performing a numerical search about this figure we found $m=0.4999$ when the Capillary number was 0.690; this result

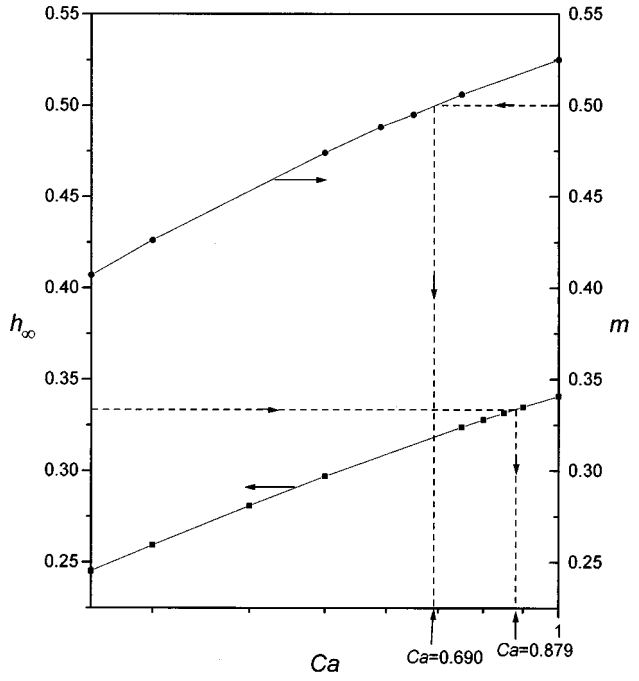

FIG. 7. Film thickness (h_∞) and film thickness parameter (m) for values of Ca between 0.2 and 1.

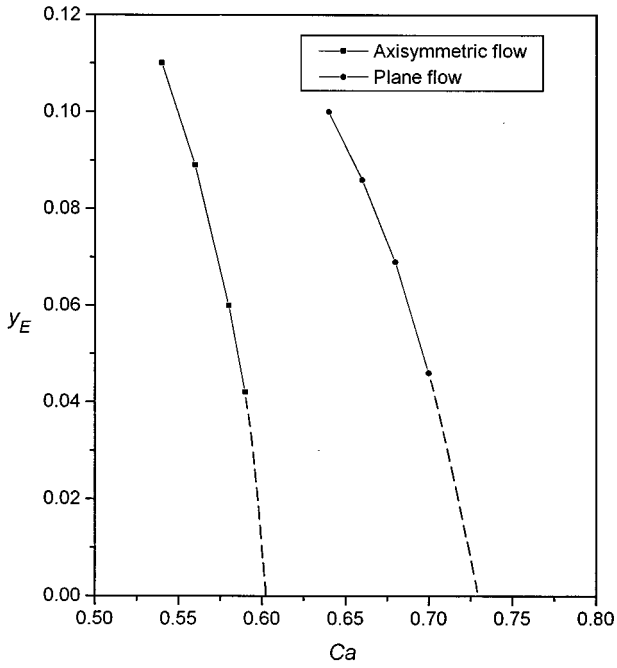

FIG. 8. Value of the y coordinate of the stagnation line located on the free surface versus Ca.

is in excellent agreement with the one reported by Martinez and Udell.[10]

On the other hand, Fig. 7 indicates for the plane case that the backflow should set in when the Capillary number is about 0.88; by carrying out a numerical exploration as before we determined 0.879 to be a more approximate value.

We have established the Capillary values at which the recirculating flow appears (or disappears) but we have not determined how the recirculation looks like in that circumstance. Figures 5(b), 5(c), and 6 indicate that the recirculating region shrinks and, at the same time, the stagnation lines recede toward the tip of the gas bubble when the Capillary number increases. Figure 8 portrays the y location of the stagnation lines versus Ca, when they are just about to reach the vertex of the gas bubble. We cannot exactly detect the Capillary number at which this situation occurs but, a simple extrapolation of the curves of Fig. 8 suggests that the stagnation lines reach the bubble vertex when the Capillary values are approximately 0.605 for the axisymmetric case and 0.730 for the plane case.

The foregoing values are smaller than those previously determined (0.690 and 0.879) for the backflow disappearance; therefore, a certain kind of recirculation must still exist when the Capillary number is in the range 0.605–0.690 for the cylindrical geometry and in the range 0.730–0.879 for the plane geometry.

Numerical explorations in the Capillary range stated in second place produced the results shown in Fig. 9; clearly, the recirculating flow region detaches from the gas–liquid interface and moves away from it as the Capillary number increases. At the same time, the recirculation weakens before vanishing at $Ca=0.879$.

Figure 9 demonstrates that two types of recirculating flow pattern exist, one is present when the Capillary number

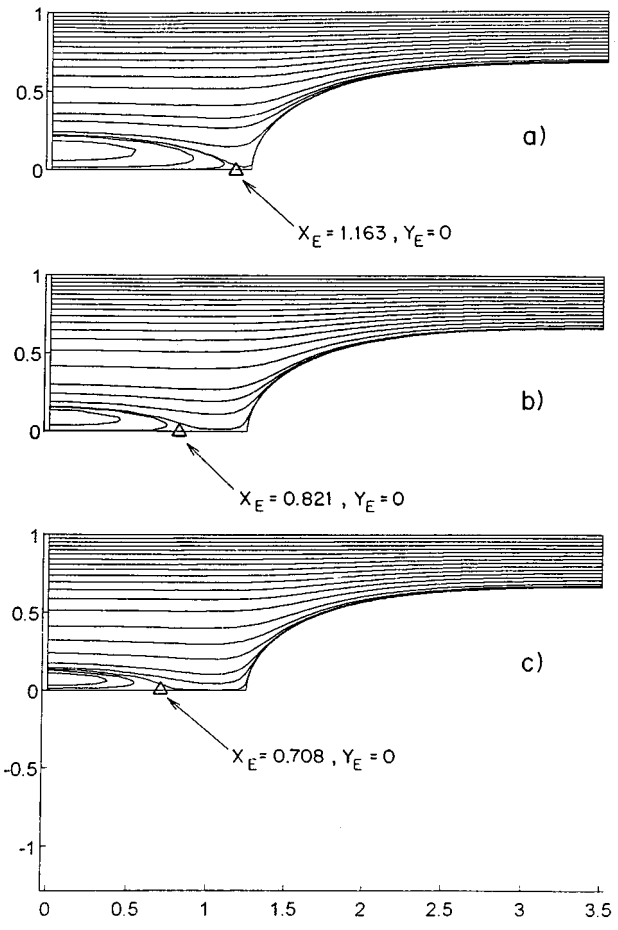

FIG. 9. Computed streamlines for plane flow: (a) $Ca=0.73$, (b) $Ca=0.80$, (c) $Ca=0.82$.

is smaller than 0.730 and is characterized by two stagnation lines—one being the mirror image of the other—located on the gas–liquid interface; a third stagnation line is situated just at the tip of the bubble. As the Capillary number increases the two stagnation lines on the meniscus move toward the third one collapsing into a single stagnation line when Ca is about 0.730. Further increases in Capillary number produce the appearance of the second recirculating flow pattern which is characterized by the presence of two stagnation lines located on the symmetry line; one is on the meniscus and the other is at the tip of the recirculating flow region which now appears separated from the gas–liquid interface.

Figure 9 portrays the streamlines for the plane case only; however, an equivalent phenomenon occurs in the axisymmetric case: For Capillary values smaller than 0.605 the recirculating flow region is characterized by a circular stagnation ring situated on the meniscus and by a stagnation point located at the bubble tip. The stagnation ring recedes toward the bubble tip as the Capillary values increase and collapses into a single stagnation point when Ca is about 0.605. When the Capillary number surpasses the value 0.605 the backflow region detaches from the interface producing a new recirculating flow pattern with two stagnation points located on the symmetry line. Finally, the flow recirculation vanishes when $Ca=0.690$.

Despite the numerous analyses performed about a gas phase displacing a confined liquid, we have found no mention regarding the second recirculating flow pattern, except for the work of Taylor[2] who in 1961 envisaged the two flow patterns just presented and qualified them as the two simplest possible types of flow when m is smaller than 0.5.

B. Inertial effects

Though inertial effects should be of little significance for the cases we are studying, we decided to evaluate them since the present methodology allows their accounting with no additional computational effort. Thus we carried out computations for fixed values of the Capillary number while the Reynolds number was varied from zero up to 70. Nevertheless, the maximum value of Re corresponding to situations feasible in practice may be much smaller depending on the value of Ca; this maximum can be estimated with the range of values summarized in Table I for both physical properties of the liquid being displaced (ρ, σ, μ) and relevant parameters of the system (d,U).

Figure 10 portrays the computed predictions of final film thickness (h_∞) versus Reynolds number for the plane case and the axisymmetric case. The results make evident that for Capillary numbers smaller than 0.01 the final film thickness does not change with Re in the axisymmetric case while a small increase is perceived in the plane case.

When the Capillary number is 0.05 or greater, the influence of the inertial forces become more evident, being the plane situation the more sensitive to the changes in Reynolds number. According to our computations, when $Ca \geqslant 0.05$ the final film thickness presents a nonmonotonic behavior, i.e., for increasing values of Re the thickness of the film first decreases, then reaches a minimum and finally increases.

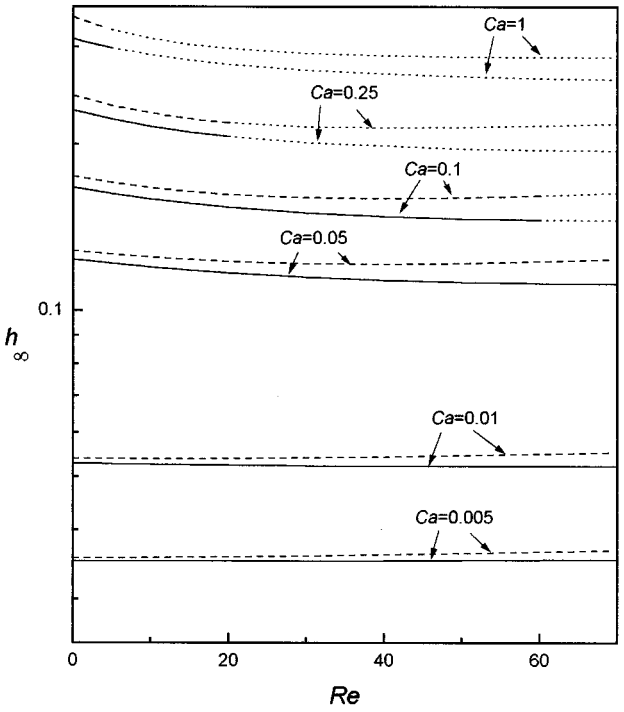

FIG. 10. Effect of Reynolds number on film thickness (h_∞) for plane flow (dashed lines) and axisymmetric flow (solid lines). Dotted lines represent situations that might not be feasible in practice.

This behavior is clearly shown in Fig. 10 when Ca is equal to 0.05, 0.1, and 0.25 for the plane case and it can also be observed in the axisymmetric case for values of Re greater than 70. The results corresponding to situations that might not be feasible in practice are shown by a dotted line in this figure.

The nonmonotonic behavior just described should be produced by a subtle balance of forces; namely, viscous, capillary, and inertial forces; however, we cannot explain the underlying mechanism that governs this phenomenon. Nevertheless, we must remark that Wassmuth *et al.*,[19] in their study of a long ''bubble'' moving through a liquid confined between parallel plates, reported final film thicknesses smaller than those obtained by Lu and Chang,[9] Reinelt and Saffman,[7] and Bretherton's theory,[3] when the Capillary number was varied between 0.015 and 0.05 and the Reynolds number was about 20. These results are in good agreement with our numerical solutions.

The distance needed by the meniscus to relax to its final film thickness also increases with the Reynolds number; the predictions are not shown here but, to give an example, we might mention the plane case for $Ca=0.1$: The film thickness attains a value equal to 1.001 of the predicted value for h_∞ at 2.6 d from the bubble leading edge when $Re=0$ and the same condition is reached at 4.4 d when $Re=40$.

The foregoing results indicate that inertial effects are of minor importance in the present problem except for the situations where the Capillary values are larger than 0.05; in addition, they demonstrate the power of the numerical method based on the simultaneous solution of the complete set of governing equations.

V. CONCLUSIONS

We simultaneously solved the flow equations and the free surface governing equations for a long bubble displacing a liquid confined either between two closely separated plates or in a cylindrical tube of small diameter. The solutions presented are for a wide range of values of the significant dimensionless parameters; viz., Capillary number and Reynolds number, and they demonstrate the quality of the numerical technique employed.

When inertial forces are negligible ($Re=0$), our results covered the whole range of Capillary values which had been numerically explored up to now with the aid of different methodologies. In addition, we extended that range by computing predictions for Capillary values as small as 5×10^{-5}.

We find excellent agreement between our film thickness and pressure drop predictions and those of Brethertons's asymptotic theory when Ca is 10^{-3} or smaller. For Capillary values larger than 10^{-3} our results reasonably agree with most of the numerical predictions already published; this agreement is particularly good with the results of Reinelt and Saffman[7] and noticeably poor with those of Lu and Chang.[7]

Streamlines fields are shown in detail for the plane case; for small values of the Capillary number the streamlines clearly show a backflow region occurring ahead of the meniscus. Just on the meniscus the recirculation zone is delimited by two stagnation lines in the plane case and by a stagnation ring in the axisymmetric case. As the Capillary number increases those limits move on the meniscus receding toward its vertex; at that point the two stagnation lines collapse into a single one and the stagnation ring collapses into a stagnation point.

If the Capillary number is increased even further, the recirculating flow detaches from the meniscus and moves away from it producing a flow pattern that in some way was foreseen by Taylor[2] 35 years ago; it appears that this flow pattern was not detected in previous analyses. Finally, when the Capillary number is large enough so that $h_\infty \geqslant 1/3$ or $m \geqslant 1/2$, the backflow region totally vanishes.

The effects produced by inertial forces on the thickness of the stationary film left behind by the moving bubble were also computed. We found a nonmonotonic film thickness variation with Re for Capillary values larger than 0.05, while the film thickness was practically insensitive to inertial forces for Capillary values smaller than 0.01.

The technique employed in this work, i.e., the simultaneous solution of the complete set of governing equations, might be promising for analyzing other free surface flow systems such as the trailing meniscus in the present problem, short bubbles or drops displacing a fluid, or the case where the interfacial properties vary locally due to the presence of surface active agents.

ACKNOWLEDGMENTS

We thank Professor D. A. Reinelt for submitting to us a copy of his results. We thank the Consejo Nacional de Investigaciones Científicas y Técnicas of Argentina (CONICET) and the Universidad Nacional del Litoral (UNL), Santa Fe, Argentina, for financial support.

[1] F. Fairbrother and A. Stubbs, ''Studies in Electroendosmosis. Part VI. The bubble-tube method of measurements,'' J. Chem. Sci. **1**, 527 (1935).
[2] G. I. Taylor, ''Deposition of a viscous fluid on the wall of a tube,'' J. Fluid Mech. **10**, 161 (1961).
[3] F. P. Bretherton, ''The motion of long bubbles in tubes,'' J. Fluid Mech. **10**, 166 (1961).
[4] J.-D. Chen, ''Measuring the film thickness surrounding a bubble inside a capillary,'' J. Colloid Interface Sci. **109**, 341 (1986).
[5] C. W. Park and G. M. Homsy, ''Two phase displacement in Hele-Shaw cells: theory,'' J. Fluid Mech. **139**, 291 (1984).
[6] J. Ratulowski and H.-C. Chang, ''Transport of gas bubbles in capillaries,'' Phys. Fluids A **1**, 1642 (1989).
[7] D. A. Reinelt and P. G. Saffman, ''The penetration of a finger into a viscous fluid in a channel and tube,'' SIAM J. Sci. Stat. Comput. **6**, 542 (1985).
[8] E. I. Shen and K. S. Udell, ''A finite element study of low Reynolds number two-phase flow in cylindrical tubes,'' Trans. ASME, J. Appl. Mech. **52**, 253 (1985).
[9] W. Q. Lu and H. C. Chang, ''An extension of the biharmonic boundary integral method to free surface flows in channels,'' J. Comput. Phys. **77**, 340 (1988).
[10] M. J. Martinez and K. S. Udell, ''Boundary integral analysis of the creeping flow of long bubbles in capillaries,'' Trans. ASME, J. Appl. Mech. **56**, 211 (1989).
[11] M. J. Martinez and K. S. Udell, ''Axisymmetric creeping motion of drops through circular tubes,'' J. Fluid Mech. **210**, 565 (1990).
[12] T. M. Tsai and M. J. Miksis, ''Dynamics of a drop in a constricted capillary tube,'' J. Fluid Mech. **274**, 197 (1994).
[13] K. J. Ruschak, ''A method for incorporating free boundaries with surface tension in finite element fluid flow simulators,'' Int. J. Numer. Methods Eng. **15**, 639 (1980).
[14] H. Saito and L. E. Scriven, ''Study of coating flow by the finite element method,'' J. Comput. Phys. **42**, 53 (1981).
[15] S. F. Kistler and L. E. Scriven, ''Coating flows'' in *Computational Analysis of Polymer Processing*, edited by J. R. A. Pearson and S. M. Richardson (Applied Science, London, 1984), pp. 243–299.
[16] M. J. Crochet, A. R. Davies, and K. Walters, *Numerical Simulation of Non-Newtonian Flow* (Elsevier, New York, 1984), pp. 222–224.
[17] W. J. Silliman and L. E. Scriven, ''Separating flow near a stactic contact line: slip at a wall and shape of a free surface,'' J. Comput. Phys. **34**, 287 (1980).
[18] B. G. Cox, ''On driving a viscous fluid out of a tube,'' J. Fluid Mech. **14**, 81 (1962).
[19] F. Wassmuth, W. G. Laidlaw, and D. A. Coombe, ''Calculation of interfacial flows and surfactant redistribution as a gas/liquid interface moves between two parallel plates,'' Phys. Fluids A **5**, 1533 (1993).